Fast optical variability of Naked-Eye Burst – manifestation of periodic activity of internal engine.

G. Beskin[1*], S. Karpov[1], S. Bondar[2],
A. Guarnieri[3], C. Bartolini[3], G. Greco[3], A. Piccioni[3]

[1]Special Astrophysical Observatory, Nizhniy Arkhyz, Karachai-Cirkassia, Russia,
[2]Institute for Precise Instrumentation, Nizhniy Arkhyz, Karachai-Cirkassia, Russia,
[3]Astronomical Department of Bologna University, Bologna, Italy,

[*]To whom correspondence should be addressed; E-mail: beskin@sao.ru.

We imaged the position of the Naked-Eye Burst, GRB080319B, before, during and after its gamma-ray activity with sub-second temporal resolution and discovered the fast variability of its prompt optical emission. Its characteristics and similarity with properties of gamma emission temporal structure suggest that it reflects the behaviour of internal engine – supposedly, a hyperaccreting solar-mass black hole formed in the collapse of a massive stellar core.

In the last several years a general picture that explains the basic observed properties of gamma-ray bursts has been developed (*1, 2*). Its main part is the formation of a compact relativistic object, a black hole or a highly-magnetized neutron star, as the result of either the collapse of the core of a massive star (*3, 4*), or the merging of two neutron stars (*5*). Such a black hole is surrounded by a massive disk of residual matter that avoided the collapse; and its accretion and interaction with the envelope leads to the launch of relativistic ejecta; its kinetic energy eventually transforms to the emission of various wavelengths. Internal instabilities or

shocks produces the gamma-ray burst itself, while the subsequent interaction of the ejecta with interstellar medium manifests as a lower energy afterglow. Temporal structure of such flares reflects both the behaviour of the "internal engine" – accreting black hole or magnetar – and the structure and dynamics of the ejecta. Activity of "internal engine" is supposedly periodical in any model, while the behaviour of the ejecta and their emission is rather stochastic and is determined by the mechanisms of conversion of kinetic energy to an internal (thermal and magnetic) one of emitting particles, by the emission mechanism itself and by the structure of the ejecta (*6,7,8,9*).

Detailed long-term study of gamma-ray burst light curves have not yet succeeded in discovery of neither periodic variations nor any other direct signatures of "internal engine" behaviour.

Detection of optical flashes accompanying the gamma-ray bursts and study of their light curves may provide significantly new information on their physics. Indeed, discovery of prompt optical emission in follow-up observations of ROTSE-I (*10*), RAPTOR (*11*), ROTSE-III (*12*) and UVOT (*13*) have lead to refinements of different GRB model details. However, it has not clarified the nature of the bursts well enough, mainly due to insufficient temporal resolution of the observations (typically worse than 10 s), that prevents the analysis of detailed structure of optical light curves and their relation to gamma-ray ones.

As a result of generic stategy of the searching for and investigation of fast optical flashes accompanying gamma-ray bursts (*14,15*) we created the FAVOR (*16*) and TORTORA (*17*) wide-field optical cameras with subsecond temporal resolution. The latter has succeeded in observing the Naked-Eye Burst (*18,19,20*). A detailed presentation and analysis of these observations are the aim of this paper.

TORTORA is a small (12 cm objective diameter) telescope equipped with image intensifier and a fast (7.5 s^{-1} frame rate, 0.13 s exposures with no gaps) TV-CCD camera which routinely monitors 24°x30° area of the sky, covering part of current Swift gamma-ray telescope field of

T_0, s	F_0, Jy	r	d	$\Delta T, s$
18.3 ± 0.3	23.2 ± 0.6	4.0 ± 0.4	-5.4 ± 4.1	8.7 ± 0.4
27.0 ± 0.3	13.4 ± 3.4	24.8 ± 8.3	-9.7 ± 4.9	9.1 ± 0.4
36.1 ± 0.2	11.4 ± 1.7	25.9 ± 7.6	-22.0 ± 17	8.3 ± 0.5
44.4 ± 0.5	15.1 ± 1.8	21.9 ± 3.3	-5.1 ± 0.2	

Table 1: Best-fit parameters for the decomposition of the light curve into 4 peaks with shape described by Kocevski (*21*) profile, shown in Figure 2. Here, T_0 and F_0 are the peak maximum positions relative to trigger time and fluxes, while r and d are the power-law indices of their rising and declining parts. ΔT is the distance between the peak and the next one.

view to catch the initial stages of gamma-ray bursts independently from gamma-ray satellite triggers. It is mounted on top of the Italian REM telescope (*17*) at La-Silla observatory (ESO, Chile).

We observed the region of GRB080319B (*18, 19*) since 05:46:22 UT, nearly half an hour before the burst (burst time is 06:12:49 UT), during the event and for several tens of minutes after its end. Since 06:13:13 UT till 06:13:20 UT REM telescope performed automatic repointing after receiving the coordinates distributed by Swift (*23*), which moved the position of the burst from the edge of the TORTORA field of view towards its center. Sample images of the burst region at different stages of the event are presented in Figure 1.

The data acquired have been processed by a pipeline including TV-CCD noise subtraction, flat-fielding to compensate vignetting due to objective design, and custom aperture photometry code taking into account non-Poissonian and non-ergodic pixel statistics caused by image intensifier. For the REM repointing time interval fluxes have been derived using custom elliptic aperture photometry code after summation of 10 consecutive frames (1.3 s effective exposure) with compensated motion of the stars, therefore no full-resolution measurements (0.13 s exposure) is available for this interval.

TORTORA acquired the data in white light with sensitivity defined by the S20 photocathode used in the image intensifier (*16*). Instrumental object magnitudes have then been calibrated to

Johnson V system using several nearby Tycho-2 (*24*) stars. A quick-look low resolution light curve (lacking the data during the REM repointing interval) has been published (*18,19*) and has been found to agree with results of other wide-field monitoring cameras which also observed this burst, such as "Pi of the sky" (*25*) and RAPTOR (*26*). Our complete full resolution light curve along with the low resolution one (after the restoring of the gap) are shown in Figure 2.

We clearly detected the transient optical emission since approximately 10 seconds after the trigger. It then displayed fast $\sim t^4$ rise, peaked at $V \approx 5.5^{\rm m}$, demonstrated 1.5-2 times variations on a several seconds time scale and decayed as $\sim t^{-4.6}$ until went below TORTORA detection limit at about hundred seconds since trigger. The gamma emission itself ended at 57th second.

The light curve clearly shows four peaks with similar amplitudes, durations and shapes. We decomposed it into four components described by a simple Kocevski (*21*) profile whose parameters are given in Table 1. We stress that distances between peaks are nearly the same within the errors, and are around 8.5 s in observer frame, which corresponds to 4.4 s in the rest frame at z=0.937 (*19*). Power spectral analysis of the plateau stage, excluding the rise and decay parts, also clearly reveals the separate peak at frequencies around this time scale (see Figure 3).

Therefore, for the first time, we have a clear detection of a periodic variations of prompt optical emission on a few seconds time scale.

We then subtracted the smooth curve, formed by four fitted peaks, from the original data and studied the residuals shown in the lower panel of Figure 2. Power spectral analysis of differerent sub-intervals of the burst revealed the signature of a periodic intensity variations during the last peak, since $T + 40$ s till $T + 50$ s, shown in Figure 4. No other intervals of the light curve show any variability in 0.1-3.5 Hz (0.3-10 s) range with power exceeding 15% before and 10% after the REM repointing. To exclude artificial nature of these variations we performed analysis of each comparison star separately in the same way as of the object. Neither comparison stars nor background display any similar periodic feature during either the whole time interval or the last

peak.

The significance level of the power density spectrum feature shown in Figure 4 is approximately 1%. The period and amplitude of the corresponding sinusoidal component, derived by means of non-linear least squares fit, are 1.13 s and 9%, respectively. The Phase Dispersion Minimization (*22*) method applied to the data (see Figure 5) also reveals the signature of a period near this time; the folded data show quasi-sinusoidal broad profile.

Such one-second periodicity is the fastest optical variability known to date for any extragalactic object.

To compare the temporal structure of optical and gamma-ray light curves we performed the cross-correlation analysis, using the plateau phase only, excluding the first and last 12 seconds of the burst both in optical and in gamma, which are obviously highly correlated (*20*) (see Figure 6). The correlation between the full-resolution optical data and the correspondingly rebinned gamma-ray one is no more than 0.5, due to high level of stochastic component in 0.1-1 s range in both optical (measurements noise) and gamma rays (actual high-frequency variability) (*27*). For the low-resolution data, with a 1.3 s binning, the correlation coefficient is, however, as high as 0.82 if the optical light curve is shifted 2 seconds back with respect to gamma-ray one (see Figure 6). Correspondingly rebinned gamma-ray data demonstrate the same four nearly equidistant peaks as optical ones.

This is the first detection of a close relation between the temporal structures of the optical and gamma-ray prompt emission. In our the case, the gamma-ray burst itself precedes the optical flash by two seconds. This result is for a period of main energy release, while the highly correlated phases of emission rise and decay have different shapes in different energy ranges.

The $\Delta t \sim 2$ s delay of optical flash relative to gamma-ray one inevitably suggests that they were generated in different parts of the ejecta, and optical photons came from the distance $\Delta R \approx 2c\Gamma^2\Delta t(1+z)^{-1} = 5.4 \cdot 10^{15}\Gamma^2_{300}$ farther from the central engine, where Γ_{300} is

the Lorentz factor in units of 300 (*1,28*).

The peculiarities we detected in Naked-Eye Burst clearly contradict models of the emission generation based on various kinds of interactions between a single ensemble of electrons and photons they generate (synchrotron or inverse Compton mechanisms) (*19,29,30*). The same can be said for a model with two shock waves where the internal forward one produces the optical emission and the internal reverse one – gamma photons (*31*), or for a relativistic turbulence model (*32,33*). On the other hand, the fast rise and similarity of durations of all four optical flashes rule out an external shock (both forward and reverse) as a source of optical emission (*34*).

At the same time, the temporal shift of the light curves, the absence of optical flux variations on 0.1-1 s in contrast to significant stochastic variability of the gamma one on the same time scale (*27*), and the strong (by thousand times) excess of optical flux spectral density in comparison to the gamma-ray one (*19*) may be explained in the internal shock with residual collisions model (*28*). In this model both high energy and optical photons are produced by a synchrotron emission of electrons on different distances from the central engine – the closer the harder the emission. The finer structure of high-energy emission is defined by the dynamics of collisions of shells with different Lorentz factors, whose kinetic energy heats the electrons by means of the shock waves. The number of colliding shells decreases with the distance (as shells merge in a collisions), which effectively smooths the optical light curve (*28*). Such a model, obviously, has its own difficulties (*35,32,33,34*), but it explains the whole set of observational data with a reasonable values of a bulk Lorentz factor $\Gamma \sim 300$, total energy $E \sim 10^{54} - 10^{55}$ erg, interstellar medium density $n \sim 0.1 - 1$ cm^{-3} and the emitting electrons Lorentz factor $\gamma_e \sim 100$ (*28,34*). The gamma-ray emission is then generated at a distance $R_\gamma < 2c\Gamma^2\tau_\gamma(1+z)^{-1} = 2.7 \cdot 10^{14}\Gamma_{300}^2$ cm (*36*), where the characteristic time scale of gamma-ray variability is $\tau_\gamma \sim 0.1$ s (*27*), while the optical one – on a $R_{opt} \sim 10^{16}$ cm distance. The latter is a consequence of obvious inequality $\Delta R < R_{opt} < 2c\Gamma^2\tau_{opt}(1+z)^{-1}$ or

$5.4 \cdot 10^{15} < R_{opt} < 1.4 \cdot 10^{16}$ cm for a characteristic optical variability time scale $\tau_{opt} \sim 4 - 5$ s (observed peaks rising time) and $\Gamma \sim 300$.

It is worth noting that the conclusion of generation of optical and gamma emission of Naked-Eye Burst at different distances from the central engine is a direct consequence of the detected shift of optical light curve with respect to gamma-ray one. It does not depend on particular mechanisms of conversion of mechanical energy to internal one of electrons nor the emission mechanisms of the latters. Taking into account the high level of similarity of optical and gamma variability on 8-9 s time scale (see Figure 6) we inevitably conclude that these variations have the same cause – namely, the cyclic variations of internal engine activity (each flash of the light curve corresponds to one of four its episodes). Obviously, it would be impossible for the relativistic ejecta itself to display similar dynamics, both spatial and temporal, in regions separated by 10^{16} cm.

Therefore, we can concluse that this is the first time in which the signature of non-stationary physical processes related to the internal engine of a gamma-ray burst was discovered in temporal structure of its prompt emission.

These cyclic variations may be the signatures of a black hole formed in a collapse of a progenitor star, surrounded by a massive hyperaccreting disk and launching the relativistic ejecta which produce the gamma-ray burst emission (*3, 37, 38*). The non-stationarity of the ejection flow is a result of non-stationary accretion – the cyclic increase (by several orders of magnitude) of the accretion rate – due to gravitational instability (*39*) in the hot inner part of the disk. The matter accumulates there due to suppression of the magnetorotational instability, driving the angular momentum transport, due to high neutrino viscosity in the inner parts of the disk. In contrast, in outer, neutrino transparent parts of the disk the development of magnetorotational instability provides "normal" accretion rate. When sufficiently high amount of matter accumulates, the gravitational instability develops in inner parts of the disk, which significantly

increase the local accretion rate. Then, after depletion of matter, the inner parts of the disk stabilize again. Such a process repeats until all the matter of the disk fall towards the black hole. As a result, the ejecta are modulated on a characteristic time scale of the matter accumulation and instability. On shorter scales, ejecta consist of separate blobs formed as a result of gravitational instability, whose collisions may result in an internal shocks.

Without going into a detailed discussion of such a model (*39*), we just note that nearly all observational properties of Naked-Eye Burst – duration of $\sim$50 s, ejecta energy of $10^{54} - 10^{55}$ erg, characteristic variability time scale in the source frame of $\sim$2.5 s – may be produced by an accretion of a one solar mass accretion disk with inner zone radius of 300 km (30 gravitational radii) onto a 3 solar masses black hole. Moreover, for the same set of parameters the $\sim$0.5 s variations in source frame, seen during the last stage of the optical transient (see Figure 4), may be interpreted as a Lense-Thirring precession or nutation (*40, 41*). As the ejecta wobbles, the line of sight crosses different parts of it with optical emission intensity varying by $\sim$10%. The non-detection of such a periodic feature in gamma-ray light curve may be due to significant stochastic component on the similar time scale (*27*).

As a result of our wide-field high temporal resolution observations of Naked-Eye Burst for the first time the fast (from one second till ten seconds) optical prompt emission variability was discovered – and this is the fastest optically variable source seen on cosmological distances. The comparison of the burst variability in optical and gamma-ray range for the first time definitely revealed the direct connection of intensity variations with the activity of central engine, which is, supposedly, a newborn stellar-mass black hole accreting from massive hyperaccreting disk.

References and Notes

1. T. Piran, *Reviews of Modern Physics* **76**, 1143 (2005).

2. P. Meszaros, *Reports on Progress in Physics* **69**, 2259 (2006).

3. S. Woosley, *ApJ* **405**, 273 (1993).

4. B. Paczynski, *ApJL* **494**, L45+ (1998).

5. D. Eichler, M. Livio, T. Piran, D. N. Schramm, *Nature* **340**, 126 (1989).

6. S. Kobayashi, T. Piran, R. Sari, *ApJ* **490**, 92 (1997).

7. F. Daigne, R. Mochkovitch, *MNRAS* **296**, 275 (1998).

8. E. Nakar, T. Piran, *ApJL* **572**, L139 (2002).

9. M. Lyutikov, *New Journal of Physics* **8**, 119 (2006).

10. C. Akerlof, *et al.*, *Nature* **398**, 400 (1999).

11. W. T. Vestrand, *et al.*, *Nature* **435**, 178 (2005).

12. S. A. Yost, *et al.*, *ApJ* **657**, 925 (2007).

13. K. L. Page, *et al.*, *ApJ* **663**, 1125 (2007).

14. A. Piccioni, *et al.*, *American Institute of Physics Conference Series*, M. Friedlander, N. Gehrels, D. J. Macomb, eds. (1993), vol. 280 of *American Institute of Physics Conference Series*, pp. 1152–1155.

15. G. M. Beskin, *et al.*, *A&AS* **138**, 589 (1999).

16. S. Karpov, *et al.*, *Nuovo Cimento C Geophysics Space Physics C* **28**, 747 (2005).

17. E. Molinari, *et al.*, *Nuovo Cimento B* **121**, 1525 (2006).

18. S. Karpov, *et al.*, *GRB Coordinates Network Circular* **7452**, 1 (2008).

19. J. L. Racusin, *et al.*, *Nature* pp. 183–188 (2008).

20. G. Beskin, *et al.*, *American Institute of Physics Conference Series*, Y.-F. Huang, Z.-G. Dai, B. Zhang, eds. (2008), vol. 1065 of *American Institute of Physics Conference Series*, pp. 251–254.

21. R. Kocevski, F. Ryde, E. Liang, *ApJ* **596**, 389 (2003).

22. R. F. Stellingwerf, *ApJ* **224**, 953 (1978).

23. J. L. Racusin, *et al.*, *GRB Coordinates Network Circular* **7427**, 1 (2008).

24. E. Høg, *et al.*, *A&A* **355**, L27 (2000).

25. M. Cwiok, *et al.*, *GRB Coordinates Network Circular* (2008).

26. P. Wozniak, W. Vestrand, J. Wren, H. Davis, *GRB Coordinates Network Circular* **7464**, 1 (2008).

27. R. Margutti, *et al.*, *2008 NANJING GAMMA-RAY BURST CONFERENCE*, Y.-F. Huang, Z.-G. Dai, B. Zhang, eds. (2008), vol. 1065 of *American Institute of Physics Conference Series*, pp. 259–262.

28. Z. Li, E. Waxman, *ApJ* **674**, 65 (2008).

29. P. Kumar, A. Panaitescu, *MNRAS* **391**, L19 (2008).

30. Y.-Z. Fan, T. Piran, *Frontiers of Physics in China* **3**, 306 (2008).

31. Y. W. Yu, X. Y. Wang, Z. G. Dai, *ApJ* **692**, 1662 (2009).

32. R. Narayan, P. Kumar, *MNRAS* **394**, L117 (2009).

33. P. Kumar, R. Narayan, *MNRAS* pp. 374–+ (2009).

34. Y.-C. Zou, T. Piran, R. Sari, *ApJL* **692**, L92 (2009).

35. P. Kumar, E. McMahon, *MNRAS* **384**, 33 (2008).

36. T. Piran, E. Nakar, *ArXiv Astrophysics e-prints* **2403** (2002).

37. A. I. MacFadyen, S. E. Woosley, A. Heger, *ApJ* **550**, 410 (2001).

38. W. Zhang, S. E. Woosley, A. Heger, *ApJ* **608**, 365 (2004).

39. Y. Masada, N. Kawanaka, T.Sano, K.Shibata, *ApJ* **663**, 437 (2007).

40. J.Hartle, K.Thorne, R.H.Price, *Black Hole: the Membrane Paradigm, ed. by K.Thorne and R.Price and D.MacDonald* (New Haven: Yale University Press, 1986), chap. 5, p. 173.

41. M. M. Reynoso, G. E. Romero, O. A. Sampayo, *A&A* **454**, 11 (2006).

42. This work was supported by the Bologna University Progetti Pluriennali 2003, by grants of CRDF (No. RP1-2394-MO-02), RFBR (No. 04-02-17555 and 06-02-08313), INTAS (04-78-7366), and by the Presidium of the Russian Academy of Sciences Program. We thank Emilio Molinari, Stefano Covino and Cristiano Guidorzi for technical help organizing TORTORA observations and for useful discussions of the results.

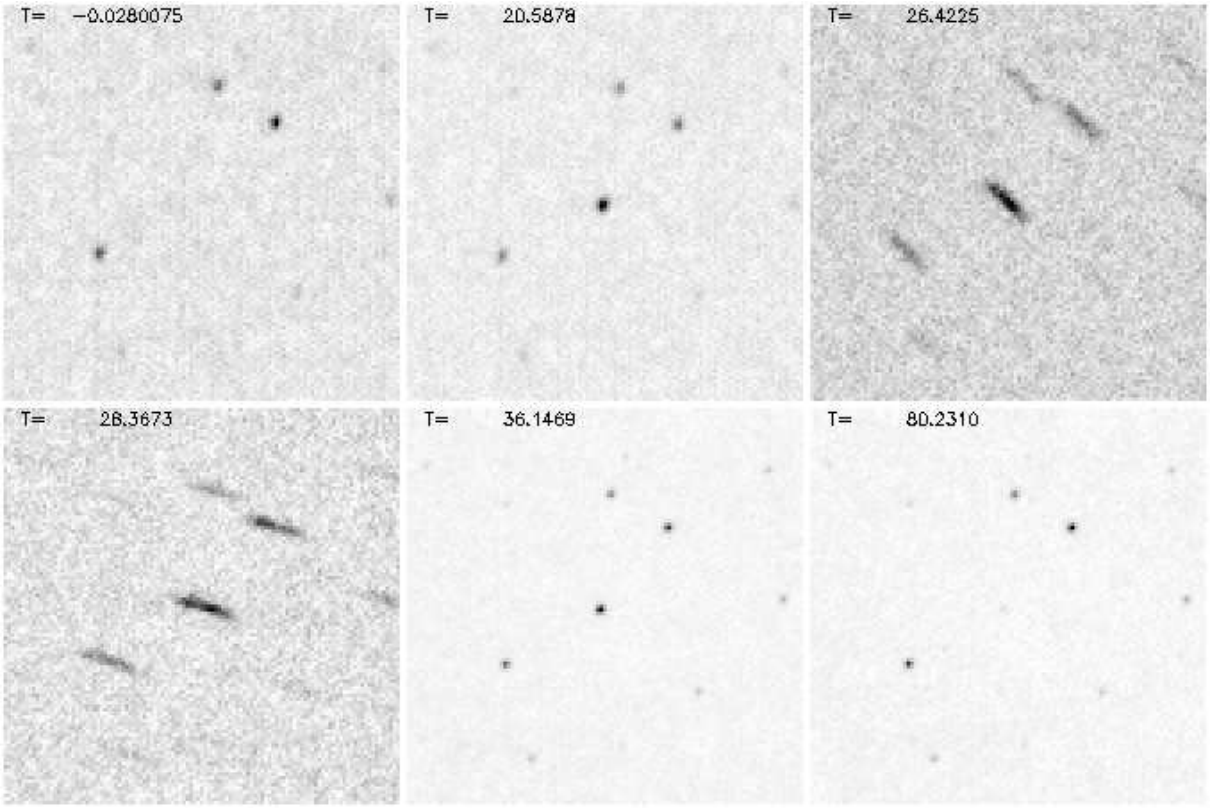

Figure 1: The development of prompt optical emission from GRB080319b as seen by TORTORA camera. Sums of 10 consecutive frames with 1.3 s effective exposures are shown for the gamma-ray trigger time ($T = 0$ s), the maximum brightness time during the first peak ($T = 20.5$ s), two middle-part moments ($T = 26.4$ s and $T = 28.4$ s), at the last peak ($T = 36$ s) and during early afterglow ($T = 80$ s) stages. Image size is 2.5 x 2.5 degrees. The third and fourth images display deformed star profiles as during this time (since $T + 24$ s till $T + 31$ s) REM robotic telescope (which has TORTORA camera mounted on top) repointed after receiving the burst information from Swift. Initially, burst position was on the edge of field of view, as a result of repointing it moved to the center of field of view, which resulted in better data quality.

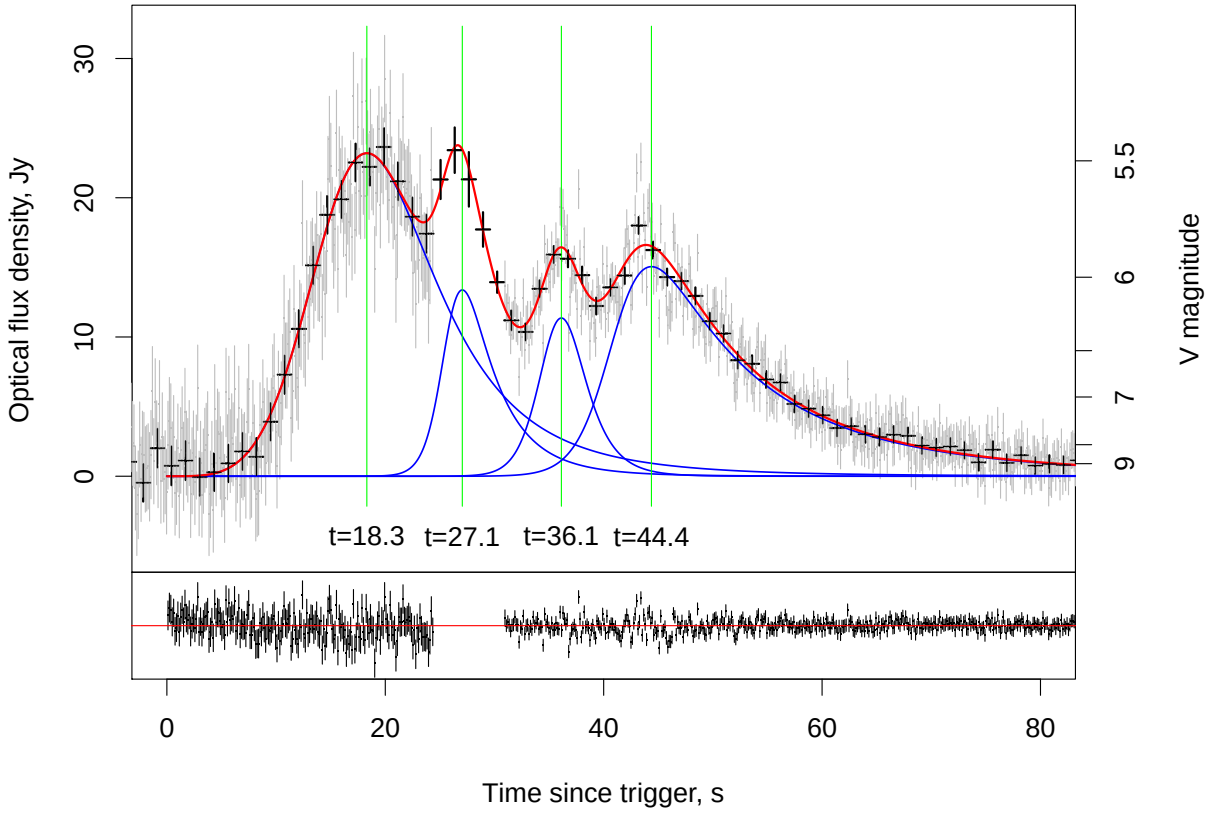

Figure 2: The light curve of GRB080319B acquired by TORTORA wide-field camera. The gamma-emission started at $T \approx -4$ s and faded at $T \approx 55$ s. Full resolution (0.13s exposure, gray lines) data are available for all duration of gamma-emission except for interval of REM telescope repointing (24.5 s $< T < 31$ s), while low-resolution ones (summation of 10 consecutive frames, 1.3 s effective exposure) – for the whole time. The light curve is approximated by a four nearly equidistant flares; lower panel shows the residuals of such approximation.

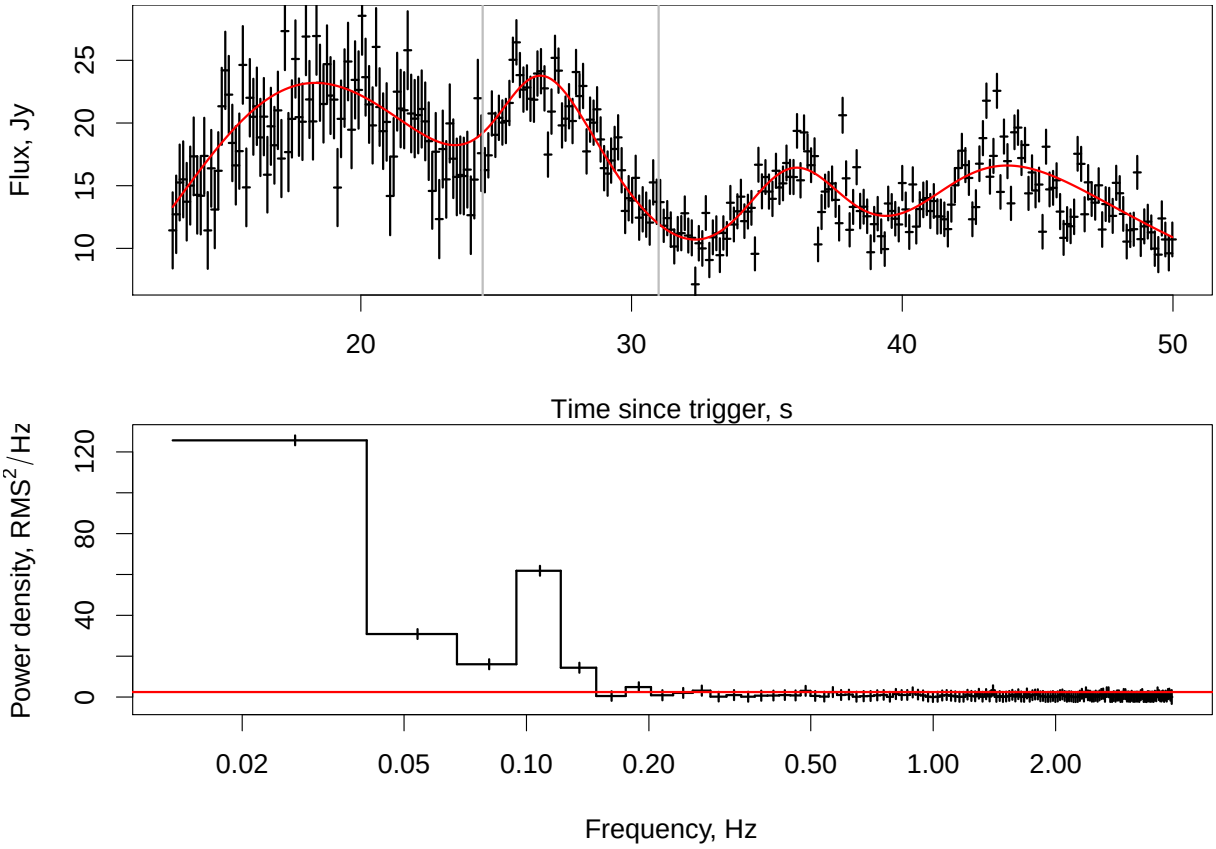

Figure 3: Upper panel – the plateau stage of the burst optical emission from $T + 13$ s till $T + 50$ s. Smooth line shows the superposition of four peaks with parameters given it Table 1. High-resolution data for a missing part (since $T + 24.5$ s till $T + 31$ s, marked with gray vertical lines) has been simulated by a white noise with a mean corresponding to the smooth curve and a standard deviation corresponding to the one around the gap. Lower panel – power density spectrum of the plateau stage. Mean noise level (horizontal line) and error bars are estimated by bootstrapping method – by generating a large number of sample time series by randomly shuffling the original light curve, what completely destroys its time structure while keeping the distibution of its values, and by studying the distribution and quantiles of resulting power densities. The feature at $\sim$9 s is clearly visible with significance level better than at least 10^-7, and corresponds to four nearly-equidistant peaks of the light curve. Low-frequency (less than 0.05 Hz) excess reflects the difference of mean intensity levels of first and second halves of the light curve.

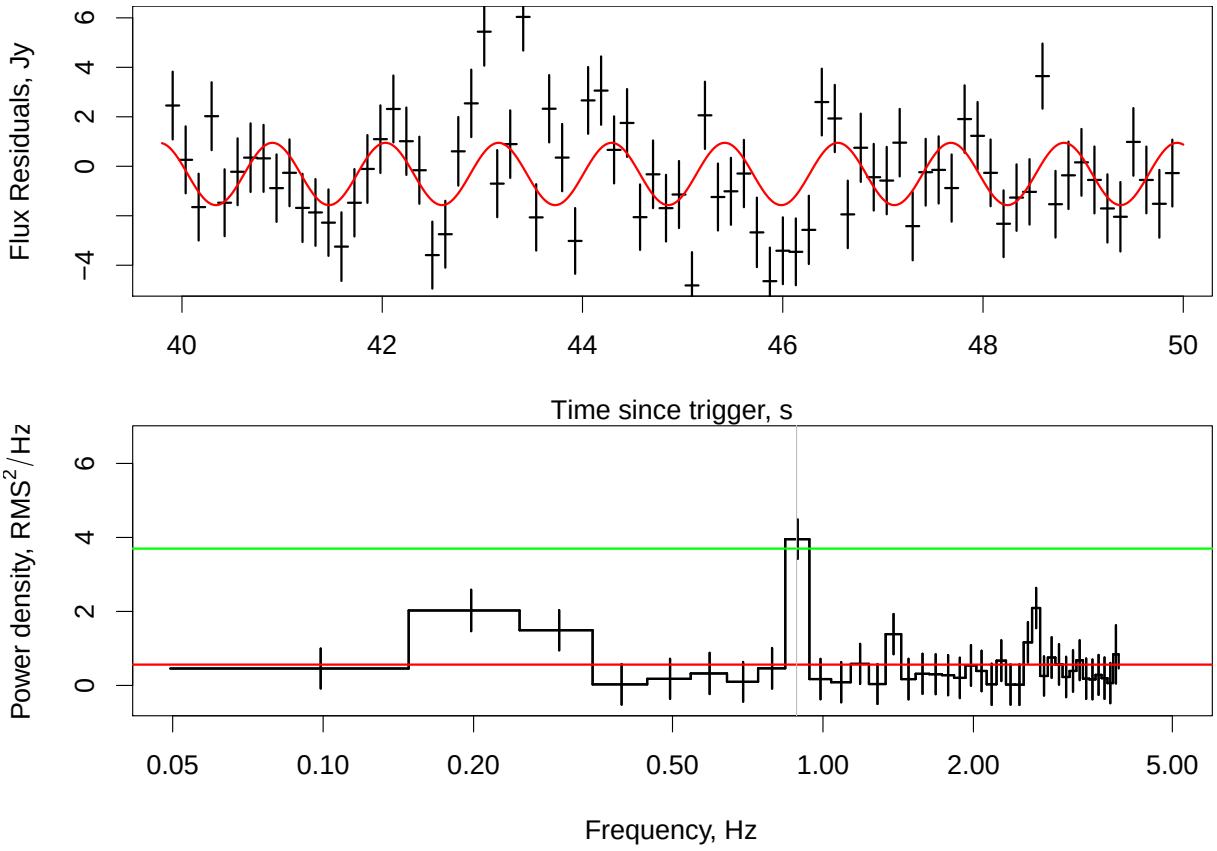

Figure 4: Upper panel – optical flux for a $T + 40$ s – $T + 50$ s interval (last peak) with the approximation shown in Figure 2 subtracted. Smooth line shows the best-fit sinusoidal approximation of the data with $P = 1.13$ s period. Lower panel – power density spectrum of this data, estimated the same way as described in Figure 3 caption. Horizontal lines represent mean noise level (lower) and a level of noise deviations with 10^{-3} significance (upper), estimated by bootstrapping number of time series from the original data set. Vertical line corresponds to the period of the sinusoidal approximation shown in upper panel, clearly coincided with the peak of power spectrum. The probability of a random appearance of a feature like the one seen in any of 39 frequency bin is ~ 0.01.

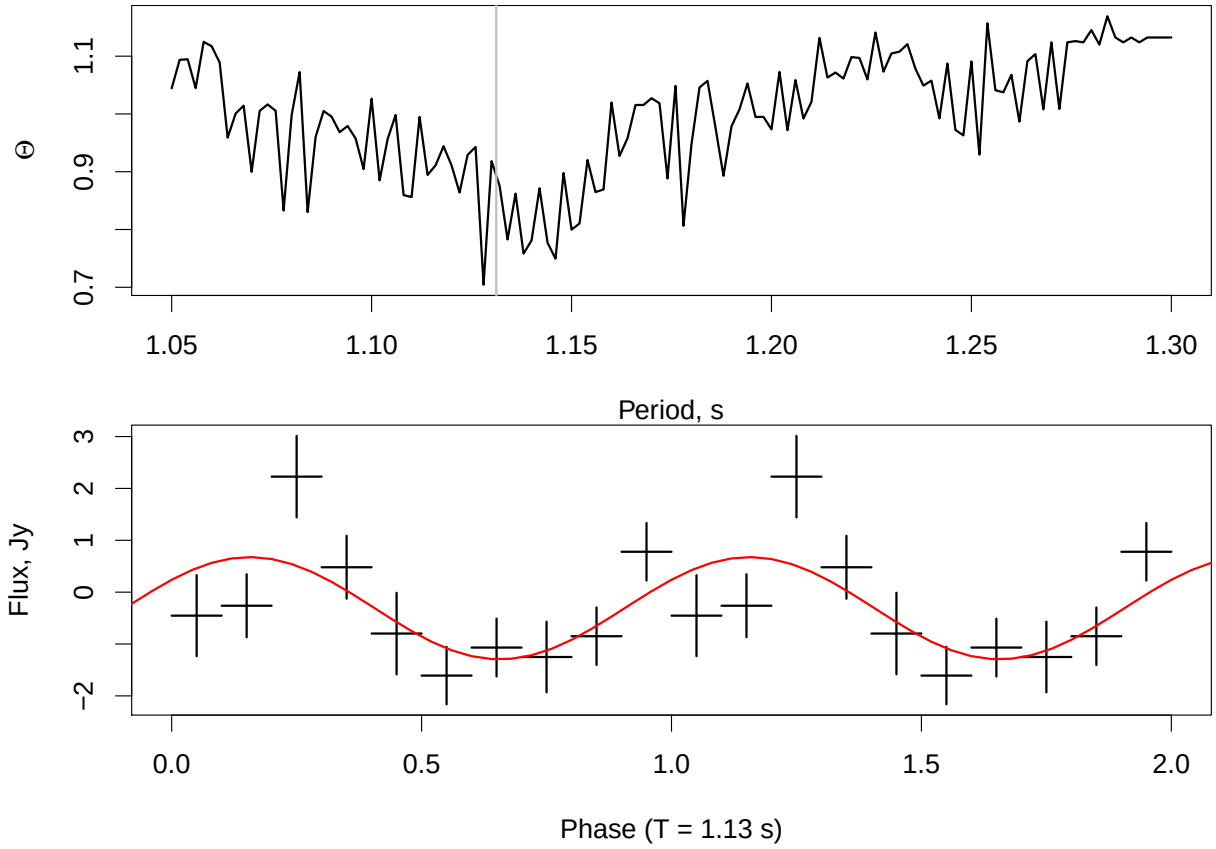

Figure 5: Upper panel – Phase Dispersion Minimization (*22*) Θ statistic for best folding period. Gray vertical line represent the $P = 1.13$ s period from sinusoidal best-fit shown in Figure 4. Bottom panel – folded mean light curve corresponding to this period, and the sine profile corresponding to the mentioned best-fit.

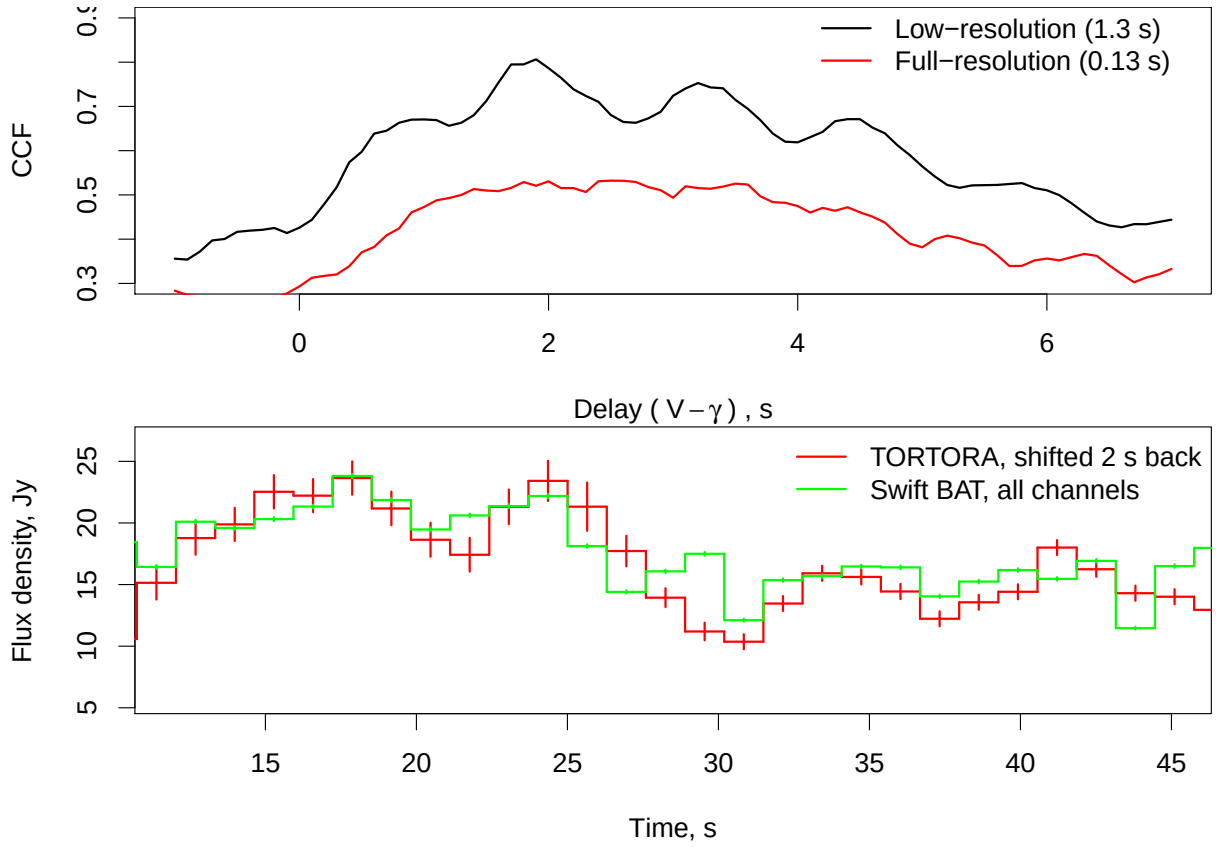

Figure 6: Upper panel – cross-correlation of the Swift-BAT gamma-ray (all energy channels) and TORTORA optical fluxes for the main (plateau) phase of the burst emission. Lower panel – TORTORA optical flux shifted back 2 seconds along with correspondingly rebinned Swift-BAT gamma-ray flux. The correlation is $r = 0.82$ with significance level of $5 \cdot 10^{-7}$. Gamma-ray curve is arbitrarily scaled and shifted for illustrative purposes.